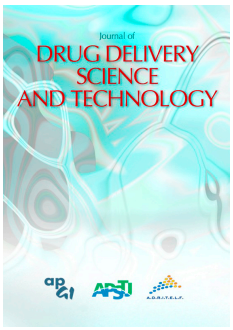

Enhanced anticancer activity of encapsulated geraniol into biocompatible lipid nanoparticles against A549 human lung cancer cells

Boris Rodenak-Kladniew, Rocío Gambaro, José S. Cisneros, Cristián Huck-Iriart, Gisel Padula, Guillermo R. Castro, Cecilia Y. Chain, Germán A. Islan

PII: S1773-2247(23)00011-4

DOI: https://doi.org/10.1016/j.jddst.2023.104159

Reference: JDDST 104159

To appear in: *Journal of Drug Delivery Science and Technology*

Received Date: 31 October 2022

Revised Date: 22 December 2022

Accepted Date: 4 January 2023

Please cite this article as: B. Rodenak-Kladniew, Rocí. Gambaro, José.S. Cisneros, Cristiá. Huck-Iriart, G. Padula, G.R. Castro, C.Y. Chain, Germá.A. Islan, Enhanced anticancer activity of encapsulated geraniol into biocompatible lipid nanoparticles against A549 human lung cancer cells, *Journal of Drug Delivery Science and Technology* (2023), doi: https://doi.org/10.1016/j.jddst.2023.104159.

Enhanced anticancer activity of encapsulated geraniol into biocompatible lipid nanoparticles against A549 human lung cancer cells

Boris Rodenak-Kladniew[1,*], Rocío Gambaro[2], José S. Cisneros[3], Cristián Huck-Iriart[4,5], Gisel Padula[2,6], Guillermo R. Castro[7,8], Cecilia Y. Chain[3], Germán A. Islan[9,*]

[1] *Instituto de Investigaciones Bioquímicas de La Plata (INIBIOLP), CONICET-UNLP, CCT-La Plata, Facultad de Ciencias Médicas, La Plata, Argentina*
[2] *Instituto de genética Veterinaria (IGEVET, UNLP-CONICET LA PLATA), Facultad de Ciencias Veterinarias UNLP, La Plata, Argentina*
[3] *Instituto de Investigaciones Fisicoquímicas Teóricas y Aplicadas (CONICET-UNLP), La Plata, Buenos Aires, Argentina*
[4] *Instituto de Tecnologías Emergentes y Ciencias Aplicadas (ITECA), UNSAM-CONICET, Escuela de Ciencia y Tecnología (ECyT), Laboratorio de Cristalografía Aplicada (LCA), Campus Miguelete, (1650) San Martín, Buenos Aires, Argentina*
[5] *ALBA Synchrotron Light Source, Carrer de la Llum 2–26, Cerdanyola del Vallès, 08290 Barcelona, Spain*
[6] *Facultad de Ciencias Naturales y Museo, UNLP, Argentina.*
[7] *Max Planck Laboratory for Structural Biology, Chemistry and Molecular Biophysics of Rosario (MPLbioR, UNR-MPIbpC), Partner Laboratory of the Max Planck Institute for Biophysical Chemistry (MPIbpC, MPG), Centro de Estudios Interdisciplinarios (CEI), Universidad Nacional de Rosario, Rosario, Argentina*
[8] *Nanomedicine Research Unit (Nanomed), Center for Natural and Human Sciences (CCNH), Universidade Federal do ABC (UFABC), Santo André, SP, Brazil.*
[9] *Centro de Investigación y Desarrollo en Fermentaciones Industriales (CINDEFI), Laboratorio de Nanobiomateriales, Departamento de Química, Facultad de Ciencias Exactas, CONICET-UNLP (CCT La Plata), La Plata, Buenos Aires, Argentina.*

Correspondance: germanislan@biol.unlp.edu.ar (G.A.I.); brodenak@med.unlp.edu.ar (B.R.-K.)

ABSTRACT

Geraniol (GOH) is a linear monoterpene alcohol found in essential oils of plants and herbs with multiple pharmacological properties, including anticancer activity. Due to its poor water solubility and volatility, GOH stability, administration, and bioavailability in physiological conditions should be improved to develop efficient carrier systems. Thus, GOH was encapsulated into nanostructured lipid carriers (NLC) as a novel strategy to improve its anticancer activity. Highly stable and lowly dispersed GOH-loaded NLC (NLC/GOH); 110 nm mean size, polydispersity index ([PDI] < 0.2), Zeta potential around -10mV, and 95% GOH encapsulation efficiency were obtained. After GOH inclusion, the crystallographic structure of NLC changed according to wide- and small-angle X-ray scattering studies. An increased *in vitro* GOH release from NLC at acidic pH (tumoral environment) after 24 h was observed. The NLC/GOH proved to be safe against blood components, adsorbed *in vitro* a thin layer of serum proteins, and preferentially interacted with human serum albumin compared with plasmatic opsonins. An efficient time-dependent cellular uptake of NLC/GOH was observed in A549 cells after 24 h. The A549 cell viability loss was increased (1.8-3.2 fold) after GOH encapsulation into NLC, which also enhanced mitochondrial membrane depolarization and cell death. Highly cytotoxic concentrations of NLC/GOH against A549 cells resulted non-toxic to normal lung fibroblasts WI-38 cells. Finally, GOH nanoencapsulation into NLC potentiated the inhibition of A549 cell migration exerted by free GOH.

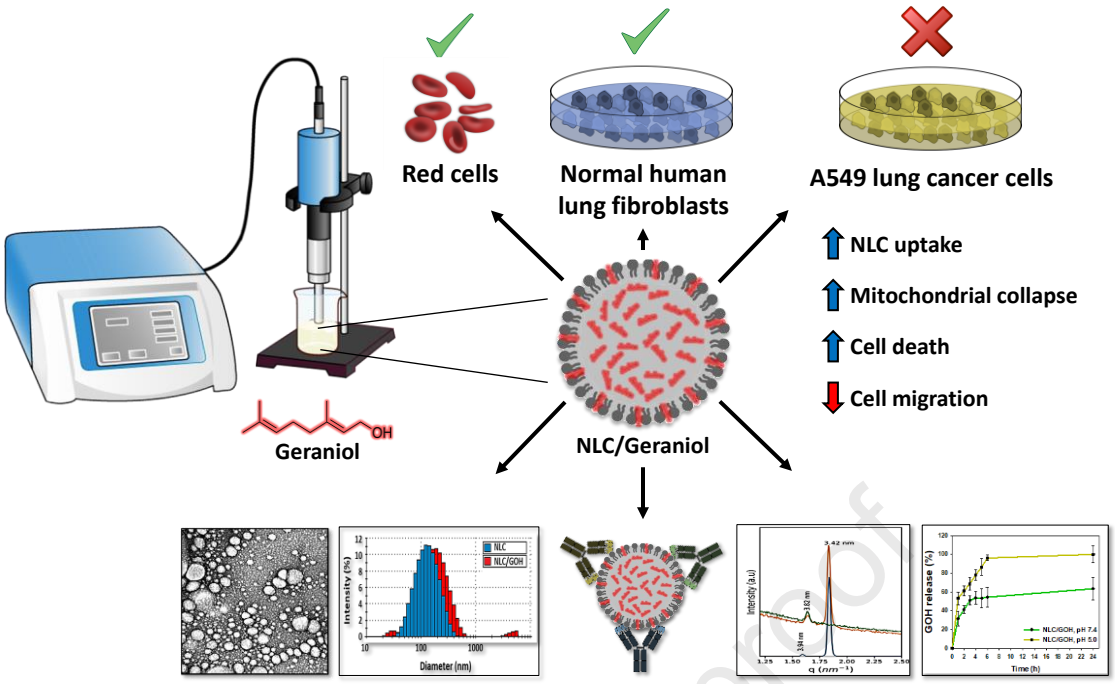

Keywords: Nanostructured lipid carriers; geraniol; drug delivery; cytotoxicity; cell migration; lung cancer cells.

INTRODUCTION

Cancer is a multifactorial disease caused by a variety of genetic and environmental factors, and the first or second leading cause of death in most countries worldwide [1]. Its incidence and mortality are rapidly rising globally because of different factors, including aging, population growth, and variations in the occurrence and distribution of the primary risk factors [2,3]. Lung cancer is a complex and very aggressive disease characterized by multiple mutations. It is classified into two main subtypes: small cell (SCLC) and non-small cell lung cancer (NSCLC), which account for 15% and 85% of total cases, respectively. By 2020, lung cancer represented the second-most commonly diagnosed cancer (11.4% of total cases) and the leading cause of cancer death (18.0%, 1.79 million deaths) by far. New promissory therapies such as immunotherapy and targeted therapy have shown relative success in lung cancer treatment because of limitations such as resistance, adverse effects, and elevated costs, resulting in poor lung cancer survival rates [4,5]. In this context, chemotherapy remains an unavoidable therapeutic option for lung cancer treatment [6,7].

Natural products have been widely screened for their anticancer properties for more than 50 years. In the last four decades, approximately one in four approved anticancer drugs were related to natural products [8,9]. Plant-derived natural products represent a rich source of anticancer drugs, including those currently employed such as etoposide, irinotecan, paclitaxel, and vincristine [9]. Monoterpenes are ten-carbon plant-derived isoprenoids with multiple

pharmacological properties that comprise chemopreventive and chemotherapeutic effects [10]. Particularly, geraniol (trans-3,7-Dimethyl-2,6-octadien-1-ol, GOH) is a linear monoterpene alcohol present in essential oils of several species like *Monarda fistulosa* (95.0%), palmarosa (93.2%), *Thymus daenensis* (75.7%), ninde oil (66.0%), rose oil (44.4%), and citronella oil (24.8%) [11,12]. Geraniol exerts anticancer activities in a wide variety of cancer cell types [13]. We have previously shown that GOH inhibits hepatocellular carcinoma cells *in vitro* and lung adenocarcinoma cells both *in vitro* and *in vivo*, deciphering some of the mechanisms of action involved [14,15]. Despite their proven anticancer activity, the use of monoterpenes has been limited in the biomedical field because of some characteristics such as high volatility, susceptibility to degradation by oxidation and isomerization, thermolability, poor water solubility, and the need for relatively high doses to reach the therapeutic window [16,17].

In the last few years, novel technologies in drug delivery have emerged to overcome these drawbacks. Nanoparticles (NPs) are nanosized colloidal systems able to deliver a wide variety of molecules, including monoterpenes. Several advantages of drug nanoencapsulation include increased water-solubility of hydrophobic drugs, improved bioavailability, controlled release, passive and/or active targeted drug delivery, and protection from degradation, elimination, or reduction of commonly associated adverse effects of anticancer drugs [18]. In addition, NPs with sizes up to 200 nm accumulate passively in the tumor microenvironment through the enhanced permeation and retention effect [19].

Solid lipid nanoparticles (SLN) are colloidal carrier systems consisting of a solid lipid core matrix stabilized by emulsifiers [20]. They were widely used for the past three decades for the encapsulation of lipophilic compounds as an alternative and more stable system than conventional colloidal carriers, such as polymeric NPs, emulsions, and liposomes [20]. However, SLN occasionally exhibit insufficient loading capacity, risk of gelation, and drug leakage of the molecular payload because of the crystallization process of lipids in the matrix over time [21]. Nanostructured lipid carriers (NLC) were thus developed as second-generation drug transporters capable of enhancing the SLN physicochemical properties. They exhibit a biphasic structure comprising both a solid lipid and liquid oil inside their matrix. The incorporation of a liquid lipid into the solid core produces a less organized lipid matrix (*i.e.*, low crystallinity), improving drug storage stability, drug loading (DL) capacity and encapsulation efficiency (EE), and promoting a controlled kinetic release profile [21,22]. Different types of NLC have been developed using monoterpene oils as dual nanostructuring and bioactive compounds [23,24]. In addition, NLC can load both hydrophobic and hydrophilic compounds, and they are composed of materials generally recognized as safe (GRAS) by the Food and Drug Administration (FDA, USA). Besides,

NLC display low *in vivo* toxicity and are easily scalable through the implementation of green technologies [21,22].

The present study aimed to develop GOH-loaded NLC as a novel biocompatible system to deliver and improve the anticancer activity of this natural isoprenoid against lung cancer cells.

2. MATERIAL AND METHODS

2.1. Materials

Geraniol (trans-3,7-Dimethyl-2,6-octadien-1-ol, GOH, molecular weight=154.25 g/mol, purity= 98%), poloxamer 188 (Pluronic® F68), tetrazolium dye MTT [3-(4,5-dimethylthiazol-2-yl)-2,5-diphenyltetrazolium bromide], and 3,3_-dioctadecyloxacarbocyanine perchlorate (DiOC18) were purchased from Sigma Chemical Co. (St Louis, MO, USA). The lipid myristyl myristate (MM) and the liquid lipid (oil) Crodamol™ GTCC-LQ were kindly donated by Croda (Argentina). Dulbecco's modified eagle medium (DMEM), Ham F12, and penicillin-streptomycin (P/S) were provided by Gibco (Invitrogen Corporation, USA). Fetal bovine serum (FBS) was purchased from Natocor (Cordoba, Argentina). Other chemicals and solvents were obtained from available commercial sources (Merck, Darmstadt, Germany), Carlo Erba (Milan, Italy), or similar brands.

2.2. Preparation of GOH-loaded/NLC

The GOH-containing NLC were prepared by homogenization with the ultra-sonication method, as previously reported [25]. Briefly, 200 mg of lipid (2.0%, w/v) was melted at 70 °C in a water bath, followed by the addition of 25 µl of liquid lipid Crodamol™ GTCC-LQ and 250 µl of GOH. In the meantime, a pre-warmed aqueous solution (10.0 mL) containing 3.0% (wt) poloxamer 188 was incorporated into the melted lipid phase. Immediately afterwards, the mixture was sonicated in an ultrasonic processor (130 W, Cole-Parmer, USA) for 10 min at 40% amplitude. The nanosuspension was then cooled at room temperature and kept at 4 °C for storage.

2.3. GOH detection

The detection of GOH was performed by ultraviolet-visible (UV–vis) spectroscopy at a λ_{max}= 240 nm. The calibration of GOH curves was performed in the range from 0.4 to 12.5 mM GOH dissolved in 75% ethanol (Figure S1).

2.4. Drug loading and EE

Drug loading (DL, %) was calculated as follows:

$$DL\ (\%) = \frac{WGOH - WNE\ (mg)}{WGOH - WNE + WL\ (mg)} \times 100 \quad (1)$$

Where WGOH = mass of GOH utilized for the NLC synthesis; WNE = mass of non-encapsulated GOH and WL = mass of lipid added to produce NLC.

The EE (%) was determined by measuring the concentration of the non-encapsulated GOH [26]. Once the NLC were prepared, a 500 µL sample was transferred to an ultrafiltration centrifugal device (MWCO 3,000, Microcon, Millipore, MA, USA) and centrifuged in a microcentrifuge (Eppendorf MiniSpin, Germany) at 10,000 ×g at 25 °C for 10 min. After centrifugation, the concentration of free GOH was determined by UV–vis spectroscopy (λ_{max}= 240 nm), and EE was calculated as follows:

$$EE\ (\%) = \frac{(Q0 - (Cr \times V))}{Q0} \times 100 \quad (2)$$

Where Q0 = initial amount of GOH; Cr concentration of GOH in the filter; V = final volume.

2.5. Particle size, zeta potential (Z-pot), and polydispersity index (PDI)

The mean size (hydrodynamic diameter, HD), distribution (PDI), and Z-pot of NLC were measured as previously described [27].

2.6. Transmission electron microscopy (TEM)

TEM analysis was performed in a Jeol-1200 EX II-TEM microscope (Jeol, MA, USA) as previously described [26].

2.7. Physical stability

After the synthesis of NPs, an aliquot was stored for six months at 4 °C in darkness and protected from light. Then, the physical stability was evaluated by analyzing variations in mean particle size, Z-pot, PDI, and EE.

2.8. Small angle X-ray scattering/Wide angle X-ray scattering (SAXS/WAXS) studies

SWAXS measurements were performed using laboratory equipment XEUSS 2.0 (XENOCS, France) with a copper target as x-ray source (0.154 nm wavelength). Patterns were registered with two photon-counting pixel x-ray detectors Pilatus 200k (DECTRIS, Switzerland) placed at 1193 m from the sample and a Pilatus 100k (DECTRIS, Switzerland) placed at 159 mm with a tilted

angle of 36°. The intensity, I(q), was recorded through the scattering momentum transfer q, where $q= 4\pi/\lambda \sin(\theta)$, 2θ is the scattering angle, and λ is the x ray wavelength. The NLC samples were placed between Kapton® tape. Measurements were done in transmission mode. SWAXS patterns were taken for 15 min each.

2.9. Release studies

Molecular release experiments were performed in 10 kDa MWCO dialysis devices (Spectra-Pors Float-a-lyzers® G2, Sigma-Aldrich, Argentina). The device was filled with 1.0 mL of the NLC formulation and immersed into a Falcon tube loaded with 30.0 mL of the release buffers: 10 mM phosphate buffer (PBS, pH= 7.4) or 10 mM acetate/acetic acid buffer system (AC- + AcH, pH= 5.0 or pH= 6.0), with 20% (v/v) ethanol at 37 °C and 150 rpm. Samples of 200 µL were withdrawn at certain time intervals, and the GOH concentration was determined at λ= 240 nm using a UV–vis spectrophotometer (TECAN Infinite 20 0 PRO, Männedorf, Switzerland).

2.10. Hemolysis studies

After written informed consent from healthy donors, heparinized venous blood was obtained from a pool of blood from 10 volunteers. Blood was placed in a 6-well plate containing Ham F12 medium supplemented with 10% FBS. Each culture was exposed to different concentrations of NLC, free GOH, and NLC/GOH according to the experimental design and kept in culture for 48 h at 37 °C with 5% CO_2. Afterwards, the mixture was centrifuged at 2500 ×g for 5 min and the pellet was discarded. Then, 100 µL of the supernatant was read at λ= 540 nm in a MultiskanTM GO spectrophotometer (Thermo Fisher Scientific, US) to determine the degree of hemolysis. Measurements were performed at 24 and 48 h. Control of 100% hemolysis was established from erythrocytes treated with 1.0% Triton X-100 whereas the negative control was obtained from erythrocytes exposed to PBS.

2.11. Static incubation with FBS

Static incubation experiments [28] were performed by mixing 200 µL of NLC/GOH dispersion with 200 µL FBS. The mixed solution was incubated for 1 h at room temperature and diluted 1/50 previous to dynamic light scattering (DLS) measurements. Control experiments were performed with FBS and NLC/GOH solutions at the same final concentrations.

2.12. Interaction with plasma proteins measured by surface plasmon resonance (*SPR)*

Measurements were carried out using an SPR Navi_ 210A (BioNavis) instrument supplied with two flow cells and operated at 725 nm incident light, 22 °C, and 10 µL/min flow rate. *In situ*

protein immobilization was achieved by a 20-min injection of 20 µg/mL immunoglobin M (IgM), 100 µg/mL fibrinogen, and 100 µg/mL human serum albumin (HSA) solutions in 10 mM sodium acetate (pH= 4.4) over the sensor chip (flow cell 1) in each three different individual experiments. Control experiments were carried out in parallel by injecting buffer solution without protein in flow cell 2. Ten-fold NLC/GOH dilutions in PBS (pH= 7.4) were injected for 10 min into the setup, followed by an injection of PBS (pH= 7.4) as running buffer and a regeneration step with 1.0% Triton X-100 (100 µL/min for 1 min) to remove the bound NLC from the sensor surfaces. The SPR response assigned to each NLC/GOH sample corresponded to the plateau of ΔϴSPR in the period between the end of the NP injection and the start of the regeneration step (around 810 s for each cycle).

2.13. Cell culture

Non-small cell lung cancer (NSCLC) A549 cells and normal human lung fibroblasts WI-38 cells were obtained from the American Type Culture Collection (ATCC). Cells were cultured in DMEM supplemented with 10% FBS (Natocor, Córdoba, Argentina) and antibiotics (1% penicillin and streptomycin; Gibco, Invitrogen Corporation, USA) in 5% CO_2 at 37 °C.

2.14. Cell viability

A549 (5×10^3) and WI-38 (8×10^3) cells were seeded in a 96-well plate and incubated for 24 h under standard conditions. Then, the medium was removed and replaced with different concentrations of blank NLC, free-GOH (dissolved in DMSO, final concentration below 0.1%), or GOH-loaded NLC in complete DMEM for 24, 48, and 72 h. Cell viability was determined by the MTT assay as previously described[25].

2.15. Measurement of mitochondrial membrane potential (MMP)

A549 cells (5×10^3) were treated with 0.1% DMSO (vehicle control), empty NLC, 1.0 mM GOH, or 1.0 mM NLC/GOH for 3 h. After washing three times with PBS, cells were stained with 5 µM rhodamine-123 in free-serum DMEM for 30 min at 37 °C in the dark. After washing three times with PBS, the intensity of fluorescence was read in a fluorescence microplate reader (Beckman Coulter DTX 880) at 488/525 nm.

2.16. Cell death

A549 cells (2×10^4) were seeded in a 24-well plate and incubated for 24 h under standard conditions. Then, cells were exposed to DMEM containing 0.1% DMSO (vehicle control), empty

NLC, 1.0 mM GOH, or 1.0 mM NLC/GOH for 24 h. Cell death was determined by trypan blue assay as previously described [29].

2.17. Cellular uptake

The cellular uptake of NPs was evaluated employing the fluorescent green dye DiOC18 (λ= 484/501 nm). A549 cells (2×10^4) were seeded in 24-well plates and allowed to adhere for 24 h. The cells were then exposed to complete DMEM containing 0.08 mg MM/mL NLC/GOH-DiOC18 for 1, 4, 8, and 24 h. Cellular uptake was analyzed by fluorescent microscopy as previously described [25,30].

In a parallel experiment, after treatment of A549 cells (5×10^3) seeded in 96-well plates, cells were washed three times with PBS, and fluorescence was determined in a microplate reader (Beckman Coulter DTX 880).

2.18. Wound healing assay

A549 cells were seeded in 24-well plates at a density of 7.5×10^4 for 24 h. Then, a wound was placed with a sterile yellow tip and the detached cells were removed after being washed with serum-free DMEM. Thereafter, the cells were exposed to 0.1% DMSO (vehicle control), free GOH (1.0 mM), or NLC/GOH (1.0 mM GOH) dissolved in serum-free DMEM. A549 cell migration was examined under an Olympus LX71 Inverted Microscope (Tokyo, Japan) at 0 and 48 h after wounding. The scratch area was determined by Image J 1.53k software (NIH, USA)[29].

2.19. Statistical analysis

Experimental data are expressed as the means ± SD. Analysis of variance (ANOVA) with a significance level of 5.0% ($p< 0.05$) followed by Fisher's least significant difference test ($p< 0.05$) was selected for comparisons of the means.

3. RESULTS

3.1. Synthesis of GOH-loaded NLC

Considering the hydrophobic nature of GOH (XLogP3-AA = 2.9), the lipid matrix composed of MM was selected for the preparation of NPs. Previous publications from our laboratory demonstrated that MM is suitable for the formation of stable colloidal NPs [25]. In concordance, a stable emulsion of GOH into NLC was obtained. Transmission electron microscopy (TEM) images demonstrated the presence of homogeneous and spherical NPs (Figure 1). The inclusion of GOH into the MM matrix seemed to produce smaller NPs than empty NLC.

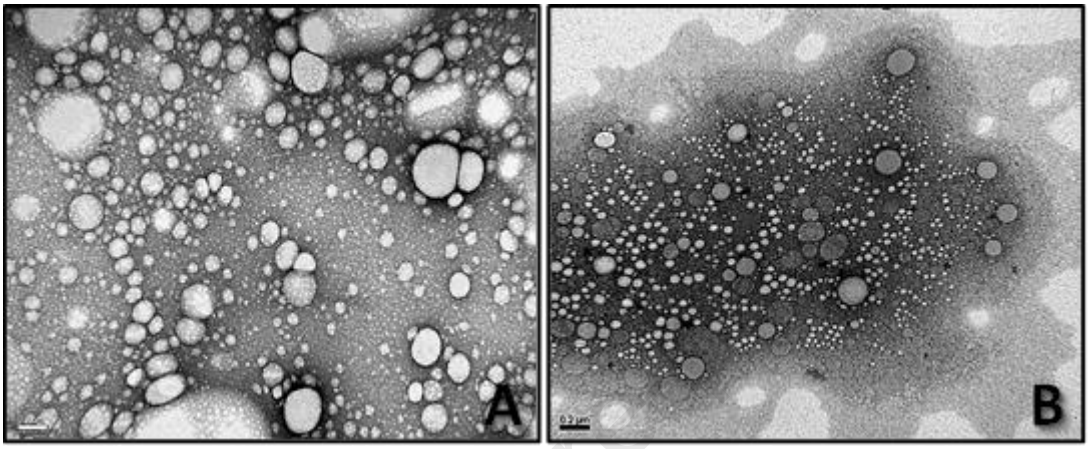

Figure 1. TEM images of NLC (A) and NLC/GOH (B).

The results observed in TEM images were corroborated by DLS analysis (Figure 2). Lipid NPs around 165 and 110 nm for NLC and NLC/GOH, respectively, were obtained. In both cases, the PDI was lower than 0.3, suggesting good compatibility for biological applications [25]. Particularly, NLC/GOH showed a PDI around 0.2, which may be attributable to the good dispersion of the emulsion, but also suggests that GOH is producing a rearrangement of the architecture in the NLC. That was evident considering that a population with sizes higher than 1000 nm observed in NLC disappeared after formulation with GOH (Figures 1 and 2A), which emphasizes the monodispersity of the NLC/GOH. A reduction in the Z-pot of NLC from -20 mV to –10 mV was observed after the inclusion of GOH, which also supports that GOH would play an important role in NLC formation. Previous reports demonstrated that SLN nanostructuration is produced in the presence of monoterpenes by reduction of the crystalline degree of the solid lipidic matrix [25]. The EE of GOH into NLC was evaluated by an indirect method and around 95% of the initial GOH was efficiently encapsulated, in concordance with the higher EE obtained for other monoterpenes such as linalool or 1,8-cineole [25,26].

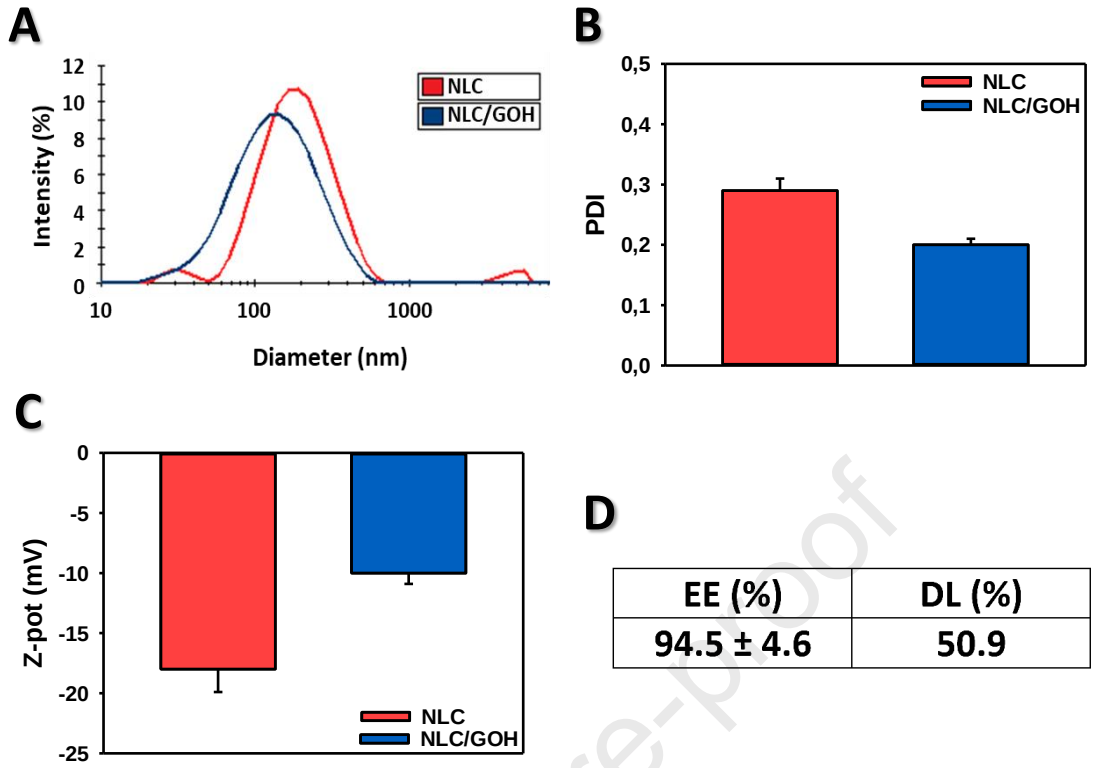

Figure 2. DLS study, GOH encapsulation efficiency (EE), and drug loading (DL). (A) Particle size, (B) Polydispersity index (PDI), (C) Z-potential (Z-pot), (D) Encapsulation efficiency (EE) and Drug loading (DL) expressed as mg of GOH/mg of myristyl myristate lipid. The results express the mean ± SD (n = 3).

3.2. Physicochemical and pharmacokinetic characterization

To elucidate the role of GOH in the structure of the lipid matrix (mainly composed of MM), SAXs/WAXs experiments were performed (Figure 3). Structural analysis was done by choosing different angular regions from SAXS and WAXS patterns. The SAXS/WAXS patterns showed the diffraction peak contribution in a selected q region from bulk MM, NLC, and NLC/GOH. The major peak positions of MM in the WAXS region (Figure 3B) expressed in terms of $d_{spacing}$ were 4.1 and 3.8 Å, corresponding to a β' polymorph [31] where $d_{spacing} = 2\pi/q$ where the long spacing distances for this form were 3.94 nm for the (001) crystallographic plane (weak peak at 1.5854 nm-1, Figure 3A) and 3.42 nm (strong peak) for (002) crystallographic plane [32]. According to WAXS patterns, the β' polymorph was the main polymorph for NLC samples, but the presence of a secondary peak at 3.82 nm at the SAXS region suggested a mix of polymorphisms due to processing. The inclusion of GOH in the composition (NLC/GOH) induced a change of polymorphisms in this secondary structure. However, this structure showed a similar WAXS pattern, where the main difference was a subtle shift of $\Delta d_{spacing} = -0.02$Å to lower angles in the first Bragg peak shown in Figure 3B. These results suggest a small change in the structure of

a subfamily of β' polymorphs, where the main differences were observed in the long spacing distances in the SAXS region.

At lower angles, it was possible to observe the structure of the copolymer in the NLC shell (**Figure 3C**). SAXS patterns showed three diffractions separated by a relation of $1, \sqrt{2}, \sqrt{3}$ which corresponded to a cubic structure [33] with a lattice parameter "a" of 10.0 nm ($d(hkl) = a / (h^2 + k^2 + l^2)^{1/2}$), where hkl are the Miller indexes and d(hkl) the $d_{spacings}$. This structure was different from the pure poloxamer 188 pattern (**Figure S2**) and previews similar systems where the structure is compatible with a lamellar organization with a period of ca. 12 nm. The main difference could be due to NLC processing, the degree of hydration of the shell after lyophilization, and interfacial effects. However, the crystallographic structure changed after GOH inclusion to the composition. The positions of the peaks in the reciprocal space relative to the position of the first peak were 1:√3:√4, characterizing a two-dimensional hexagonal network [33]. The lattice parameter of this hexagonal arrangement, "a", was calculated from the distance between the reflections: $d(hk) = (2/\sqrt{3})a / (h^2 + k^2 + hk)^{1/2}$, which gives a value of 14.4 nm. Since GOH is a small alcohol (terpenoid) that can act as a surfactant and interact with the lipidic phase through -OH moieties and with the poloxamer 188 as well, these results suggest that GOH could be distributed along all the NLC structures.

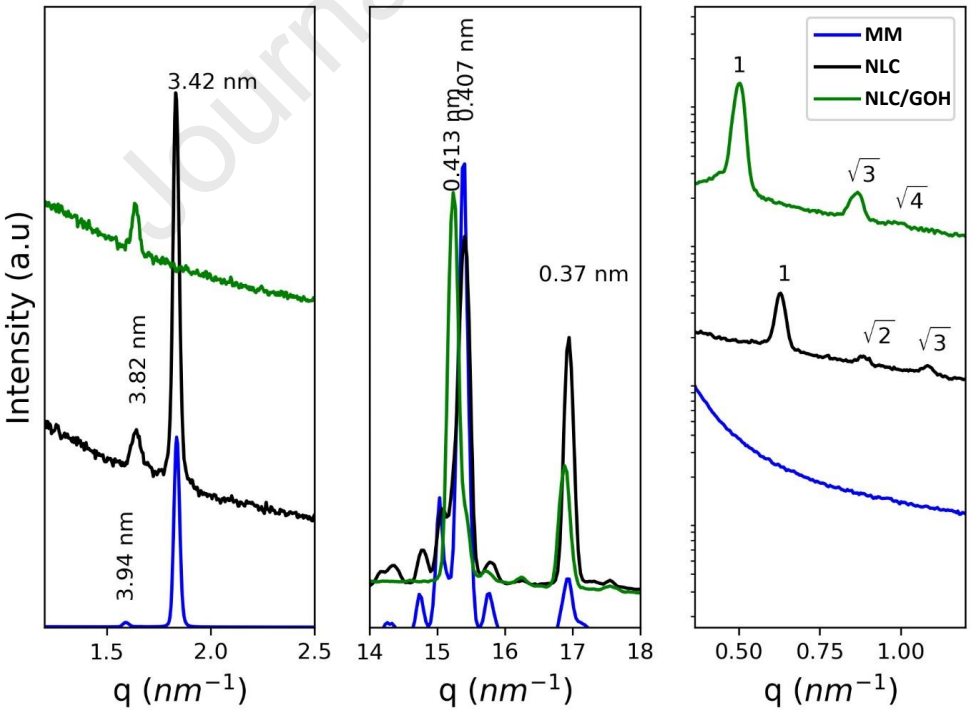

Figure 3. SAXS/WAXS patterns for MM, NLC, and NLC/GOH. (A) SAXS/(B) WAXS patterns for MM, NLC, and NLC/GOH samples; (C) SAXS at low angle patterns for MM, NLC, and NLC/GOH samples. The y-axis is plotted in a log scale for better visualization.

On the other side, the kinetic release of GOH from the NLC matrix was studied (**Figure 4**). The tumor-specific pH response was evaluated at pH= 7.4 to simulate the physiological environment, as well as at pH 5.0 and 6.0 which could be related to endosome pH and the acidic conditions produced by tumoral cells, respectively [34,35]. The free diffusion of GOH across the dialysis membrane was checked at the three pHs. A pH-dependence of the GOH released from NLC was observed in the acidic and neutral conditions. Around 60% of the total encapsulated GOH was released from NLC at neutral pH, while 100% was released at both acidic pHs after 24 h incubation. The formulation exhibited a typical bi-phasic release profile at the tested pHs. An initial strong burst release was produced at pH 5.0 and 6.0 during the first 6 h. However, that burst release was almost 2-times lower at neutral pH than at acidic pHs. At pH 7.4, the kinetic was started with a 50% release of the cargo during the first 3 h. After the bursting stage, the NLC released GOH in a sustained manner for the next hours in all conditions. This is an important finding which may become a useful tool for actively targeted therapies to tumoral environments, reducing the systemic circulation of the chemotherapeutics under physiological conditions [36]. Moreover, intracellular GOH release into acidic endo-lysosomes would be favored following cell uptake by the endocytic pathway, which was described as the main mechanism of internalization for lipid nanoparticles of similar characteristics [37].

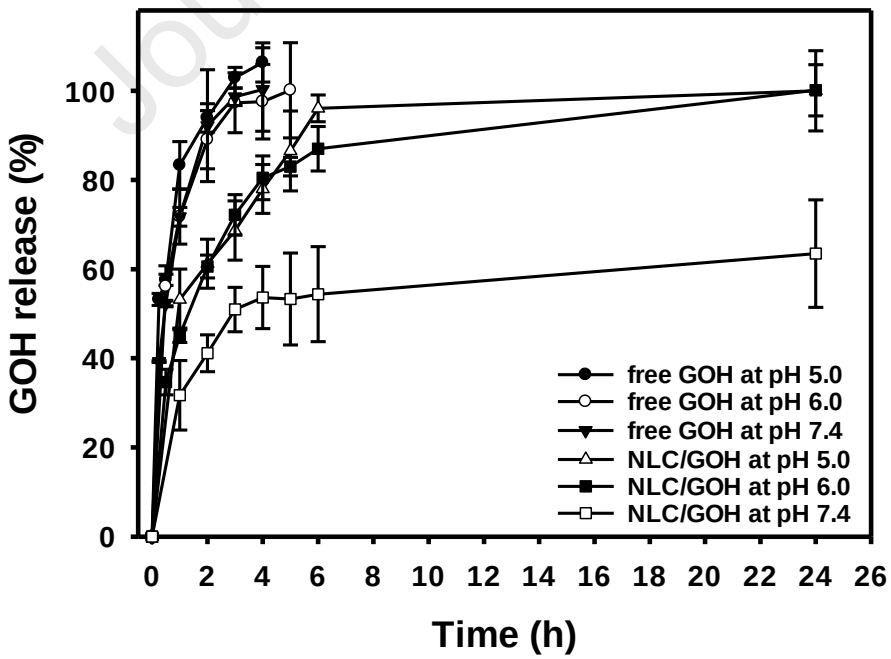

Figure 4. GOH release from NLC/GOH at pH 7.4, 6.0, and 5.0. The values express the mean ± standard error of the mean (n = 3).

The stability of the NLC/GOH is a critical point to ensure the reproducibility and potential application of the formulation. Stability was followed in terms of EE, size, PDI, and Z-pot of NLC for 6 months after storage at 4 °C (Figure 5). As expected for this kind of systems, no changes in the studied parameters were observed, suggesting that NLC/GOH were stable during this period. Despite the low Z-pot values observed in the NLC/GOH formulation, the high stability could be explained by the stabilization with a non-ionic surfactant. The steric groups of the Poloxamer 188 could stabilize the formulation and avoid the agglomeration of NLC after storage [38,39]. Furthermore, it was reported that NPs stabilized with a non-ionic surfactant usually show high stability, even if Z-pot values do not reach the critical ±30 mV [40].

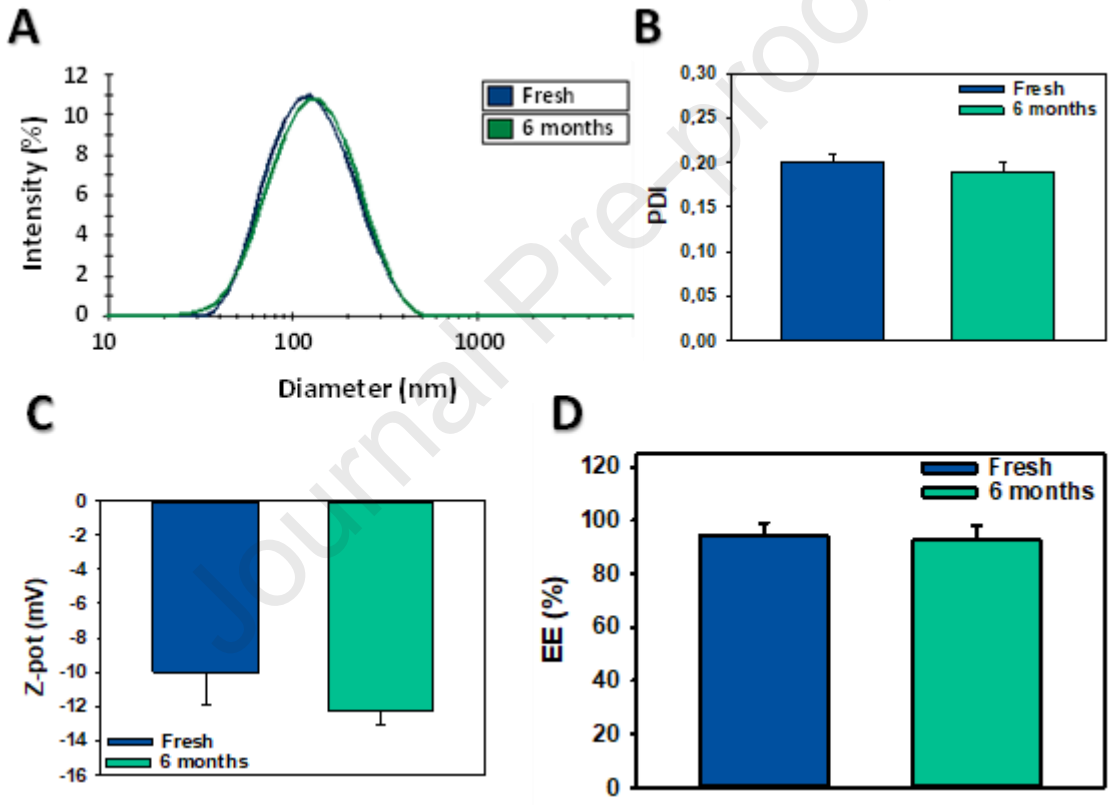

Figure 5. Stability of the NLC/GOH formulation over time. Stability of the NLC/GOH after 6 months stored at 4 °C. (A) Particle size, (B) Polydispersity index (PDI), (C) Z-potential (Z-pot), (D) Encapsulation efficiency (EE). The results express the mean ± SD (n = 3).

3.3. Hemocompatibility assays

As a first approach to detecting the potentially harmful effects of the NLC, the hemotoxicity of the NLC/GOH was assayed (Figure 6). Considering intravenous administration as an NLC potential route, the interaction with erythrocytes became a relevant point to determine the safety of NPs [41]. The ISO/TR 7406 established that biomaterials that cause a hemolytic ratio

< 5% could be considered safe for human applications [42]. The analysis of blood samples exposed to NLC, free GOH, and NLC/GOH revealed negligible hemolysis (less than 3% for all cases) at 24 h. Similarly, a reduction of hemolysis after encapsulation of 2.0 mM GOH into NLC ($p < 0.05$) after 48 h exposure was observed. This effect may be attributed to the controlled release of GOH from NLC, which exposed erythrocytes to lower monoterpene concentrations, particularly during the first stages of contact.

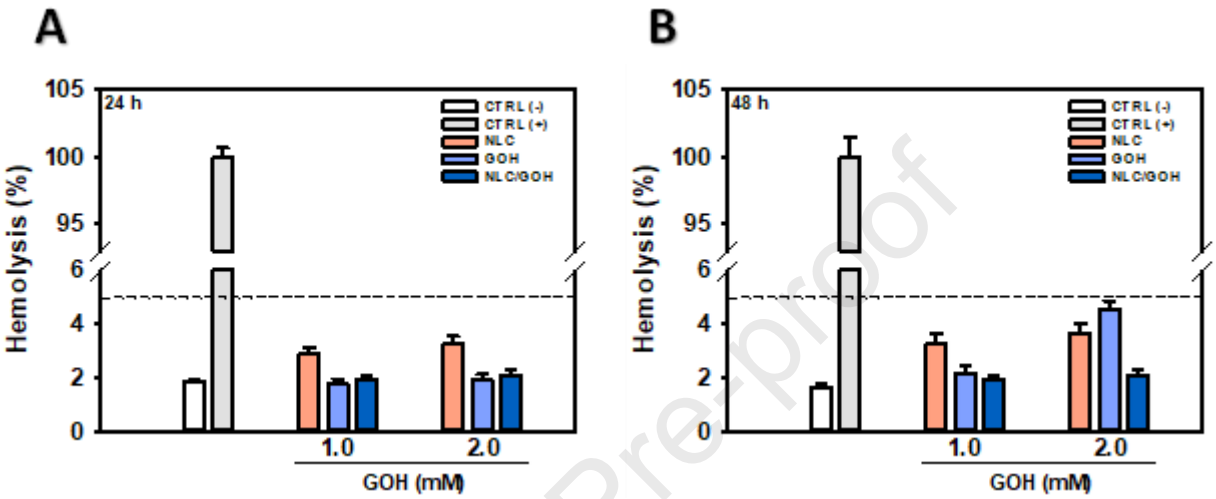

Figure 6. Hemolysis of empty NLC, free GOH, and NLC/GOH. Hemolysis of 1.0- and 2.0-mM GOH, and equivalent quantities of empty NLC and NLC/GOH, was evaluated after 24 (A) and 48 h (B) incubation. The results express the mean ± SD (n = 3). C (-): untreated cells; C (+): 1.0% Triton X-100-lysed erythrocytes.

3.4. Formation of protein corona and interaction with selected plasma proteins

As protein corona can affect the plasmatic clearance and target properties of nanovehicles, we investigated by DLS if the mean DH of NLC/GOH changed after incubation with FBS under static conditions. Before incubation, the NLC/GOH suspension exhibited a unimodal and centered DLS distribution at DH = 116 ± 2 nm, and the FBS solution a trimodal DLS distribution, with peaks centered at 9 nm, 30 nm, and 200 nm due to typical protein sizes (**Figure 7A**). After 60 min of exposure to FBS, a single peak centered at DH ≈ 125 nm ± 3 was detected (**Figure 7B**). The ~ 9 nm shift in DH found in NLC/GOH incubated for 1 h with FBS was compatible with a thin layer of ~ 4.5 nm, which can be ascribed to a single layer of proteins [43] of low- and medium- DH serum proteins, whose peaks disappeared after incubation. These results also verified that no clustering processes occurred in the developed nanoformulations, in comparison with other lipid NPs of around the same size, where a ~ 200 nm shift was found after incubation with FBS under the same conditions [28].

To investigate the interaction of NLC/GOH and selected plasma proteins with different effects on circulation times, SPR studies were performed. With this aim, three proteins with low- and medium-DH [44] were immobilized onto a gold surface, and subsequently, NLC/GOH suspensions were injected over the functionalized sensor chip. Thus, HSA (DH= 7 nm), fibrinogen (DH= 22 nm), and IgM (DH= 25 nm) were injected onto Au sensor surfaces, causing a clear change in SPR peak angular position (ΔΘ of 0.25, 0.41, and 0.43 degrees, respectively), verifying the physical adsorption of the proteins. To study the biomolecular interaction, NLC/GOH suspensions were injected over the functionalized surfaces (a schematic sensor surface is shown in Figure 7D), yielding the sensorgrams that are shown in Figure 7C. The SPR signals corresponding to the interactions between NLC/GOH and IgM (or fibrinogen) appeared to be comparable to or lower than those established with the control surface. However, ΔΘ of the interaction of NLC/GOH and HSA (ΔθSPR ~0.07) was higher than the control experiment. This finding is encouraging, as HSA is a well-known disopsonin (*i.e.,* a protein that enhances circulation time) as opposed to the effect exerted by the opsonins IgM and fibrinogen, which may trigger the clearance of the nanovehicles from the body [45].

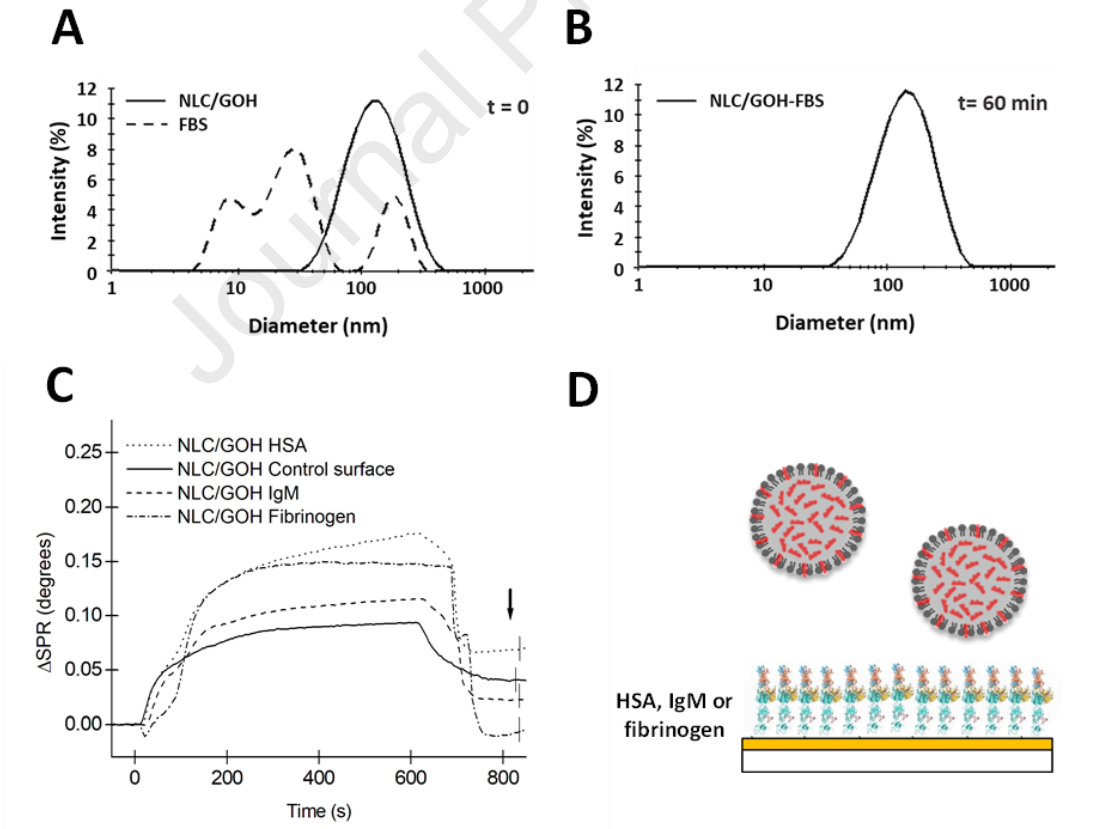

Figure 7. Interaction of NLC/GOH with plasma proteins. Formation of protein corona and interaction with selected plasma proteins. (A) Dynamic light scattering (DLS) distributions of NLC/GOH and FBS at t = 0 min. (B) NLC/GOH–protein corona at t = 60 min. (C) Change in SPR peak minimum angular position as a function of time during the interaction of NLC/GOH and selected proteins (fibrinogen, HSA, or IgM). Control surfaces corresponded to sensor surfaces without protein. The arrow indicates the time point where the interaction was analyzed. (D) Scheme of the sensor platform design used in SPR experiments.

3.5. Cellular uptake

The success in terms of efficient delivery and bioavailability of the encapsulated agents into therapeutic nanoparticles strongly depends on the cellular uptake profile of the nanocarrier. The process of cellular uptake is a multistep event that starts with the adhesion of NPs to the cell surface, followed by their internalization by distinct mechanisms which depend on several factors, including charge, shape, size, and surface of NPs [46]. The time course uptake of NLC/GOH/DiOC18 in A549 cells was analyzed (**Figure 8**). As observed qualitatively in living cells by fluorescent microscopy, the cellular uptake takes place in a time-dependent way in the evaluated period (**Figure 8A**). The images suggest that NPs would be predominantly distributed through the cytoplasm. The kinetic uptake profile observed in NLC/GOH/DiOC18 was confirmed quantitatively by spectrophotometric determinations (**Figure 8B**). Nanoparticle uptake increased over time between 1 and 24 h exposure. These results suggest that A549 cells were not exposed to saturation levels of NPs under our conditions since no decline or plateau in uptake levels was noted.

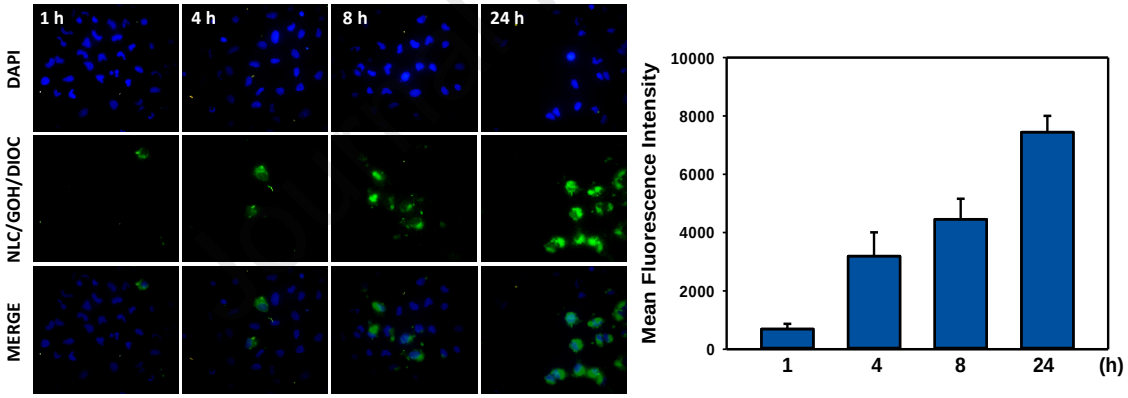

Figure 8. Cellular uptake of NLC/GOH in A549 cells. Time-dependent uptake (1, 4, 8, and 24 h) of DiOC18-loaded NLC/GOH by A549 cells. (A) Fluorescence microscopy images of the cellular uptake of labeled NPs (green). Nuclei were stained with DAPI (blue). Representative images of triplicate experiments are shown (600 ×). (B) Quantitative analysis of DiOC18-loaded NLC/GOH cellular uptake in A549 cells measured spectrophotometrically. The results are the mean ± SD (n = 6).

3.6. Anticancer activity

Geraniol is a monoterpene whose anticancer activity has been extensively explored in several types of cancer [47,48]. Aiming to analyze the potential benefits of GOH encapsulation, the cytotoxic activity of free and GOH-loaded NLC was studied in two cell models: lung cancer (A549) and normal lung fibroblasts (WI-38) cells. Cells were exposed to increasing concentrations

of free or encapsulated GOH (0.25 – 1.5 mM) and equivalent quantities of empty NLC for 24, 48, and 72 h, and an MTT assay was carried out (Figure 9). As expected, both free and encapsulated GOH inhibited A549 cell viability in a dose- and time-dependent manner (Figures 9A-C). After 24 h exposure, the encapsulation of GOH decreased cell viability from 77.1 to 58.7% at 1.0 mM and, most substantially, from 71.2 to only 7.8% at 1.5 mM (Figure 9A, $p < 0.001$ in both cases). This improvement in GOH cytotoxic activity after nanoencapsulation was also evident at lower concentrations, where cell survival significantly decreased from 0.5 mM GOH after 48 and 72 h exposure ($p < 0.001$, Figures 9B-C). In all cases, empty NLC did not result cytotoxic for A549 cells (cell viability greater than 70%) [49]. The enhancement of GOH activity after encapsulation against A549 cells could be attributable to a sum of factors, including prolonged stability of GOH at 37 °C in the cell culture medium, increased GOH permeation, a more prolonged period of cytotoxic concentrations of GOH due to an NLC-mediated controlled release, and potential evasion of GOH expulsion/metabolism favored by NLC [50–52].

One of the main goals of cancer therapy is to strike tumor cells avoiding, or minimizing, adverse toxic effects on normal tissues. For that reason, NLC/GOH cytotoxicity on WI-38 normal lung fibroblasts was evaluated [29]. As observed in Figure 9D-F, NLC/GOH were non-toxic in the range of concentrations explored for up to 72 h. These results, together with hemocompatibility studies, suggest that the developed NLC/GOH formulation is a safe and potent enhancer of GOH anticancer activity.

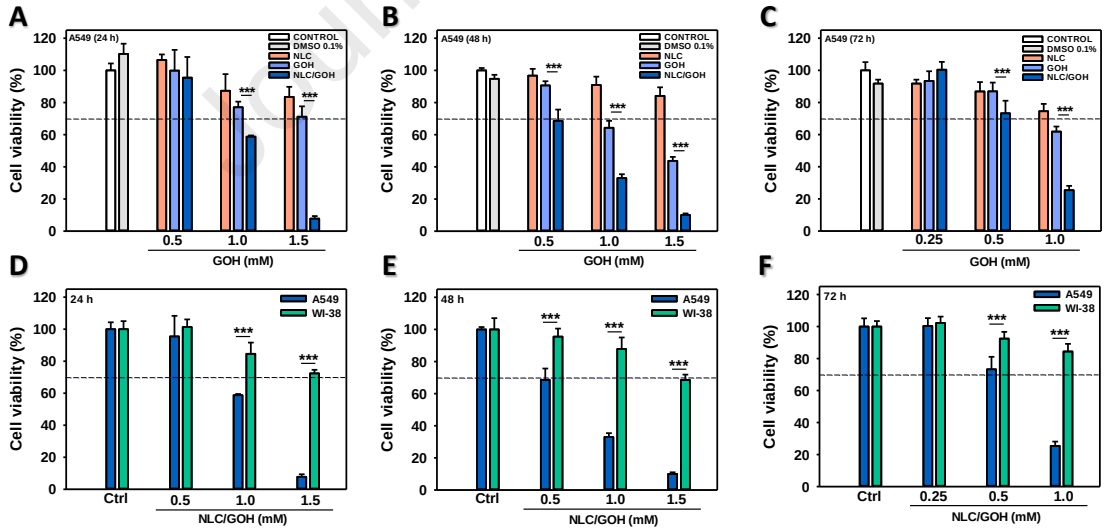

Figure 9. Cytotoxicity of NLC/GOH on lung cancer (A549) and normal lung fibroblasts (WI-38) cells. (A-C) A549 cells were exposed to increasing concentrations of free GOH, empty NLC, and NLC/GOH, and cell viability was assayed by MTT after 24 (A), 48 (B), and 72 h (C) incubation. Free GOH was dissolved in DMSO (0.1% v/v). (D-F) Cell viability of WI-38 cells (green bars) exposed to increasing concentrations of NLC/GOH after 24 (D), 48 (E), and 72 (F) h exposure. Results are compared with those of A549 cells obtained under the same conditions (blue bars). Results are expressed as the mean ± SD (n = 6), (***) $p < 0.001$. The dotted line indicates 70% viability; below that, the formulation could be considered cytotoxic.

To shed light on some mechanisms involved in A549 cell growth inhibition mediated by NLC/GOH, cell death (Figure 10A) and mitochondrial membrane depolarization (Figure 10B) were evaluated. As observed in Figure 10A, cell death was significantly increased from 1.1% in control cells to 8.1% in 1.0 mM-GOH treated cells ($p < 0.001$), whereas 1.0 mM NLC/GOH increased cell death up to 19.2% ($p < 0.001$). Mitochondrial metabolism is commonly altered in cancer cells [53]. Mitochondria are considered the major cellular energy-producing organelles but also their suicidal weapon store. A wide variety of death signal transduction pathways converge on mitochondria to produce the permeabilization of the mitochondrial membrane, leading to the cytosolic release of pro-apoptotic proteins such as cytochrome C [53]. Triggering cancer cell death by promoting mitochondrial membrane permeabilization or by inhibiting tumor-specific alterations of the mitochondrial metabolism may result in promising therapeutic attempts. Here, we found that free GOH (1.0 mM) decreased MMP by 19.2% ($p < 0.05$) whereas GOH-loaded NLC augmented MMP loss up to 34.5% ($p < 0.05$) compared with control cells (Figure 10B). These results are in line with the cell death increase observed previously and suggest that NLC/GOH could be exacerbating the pro-apoptotic activity of GOH previously reported [14,15].

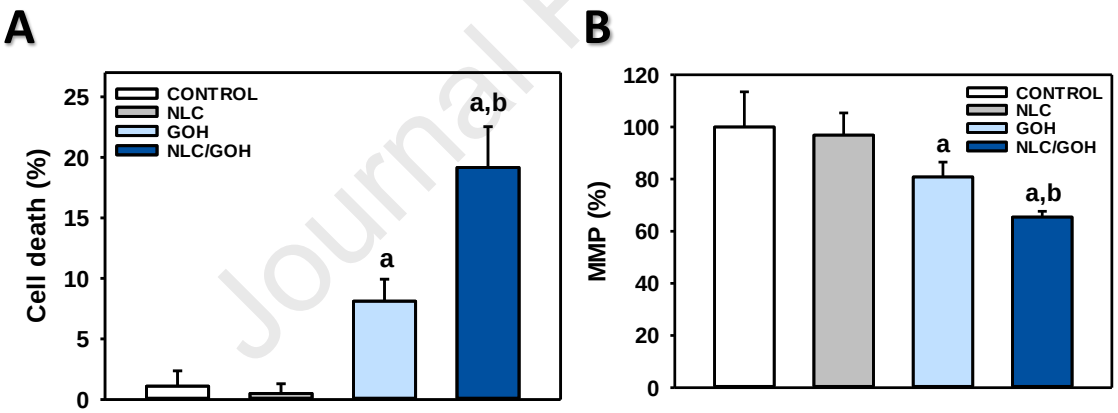

Figure 10. Encapsulation of GOH increases MMP depolarization and cell death in A549 cells. (A) Cells were incubated with 0.1% DMSO (vehicle control), 1.0 mM free GOH, or 1.0 mM NLC/GOH for 24 h, and cell death was analyzed by trypan blue staining. (B) Cells were incubated with 0.1% DMSO (vehicle control), 1.0 mM free GOH, or 1.0 mM NLC/GOH for 3 h and then stained with rhodamine-123. Data are presented as the mean ± SD (n=4). (a) $p < 0.05$ vs. control; (b) $p < 0.05$ vs. free GOH.

Another aspect to be considered is cell migration, which is a hallmark of cancer invasion and tumor metastasis. In addition, lung cancer is among the most common primary cancers leading to metastasis [54]. Therapeutic systems harboring both cytotoxic and anti-metastatic activities are ideal candidates for lung cancer treatment. To increase the knowledge of both the anti-cancer mechanisms of GOH and the potential benefits of its encapsulation in NLC, the effect on cell migration was studied through the wound healing assay (Figure 11). We found that after

48 h, GOH significantly suppressed A549 cell migration and reduced the wound closure to 28.8% as compared with the 65.7% observed in control cells (**Figure 11b**, p< 0.001). Incorporation of GOH into NLC increased the inhibitory activity on cell migration, reducing the wound closure to only 8.6% (**Figure 11b**, p< 0.001). These results suggest that GOH exerted antimetastatic effects on A549 lung cancer cells while GOH encapsulation definitively improved its activity.

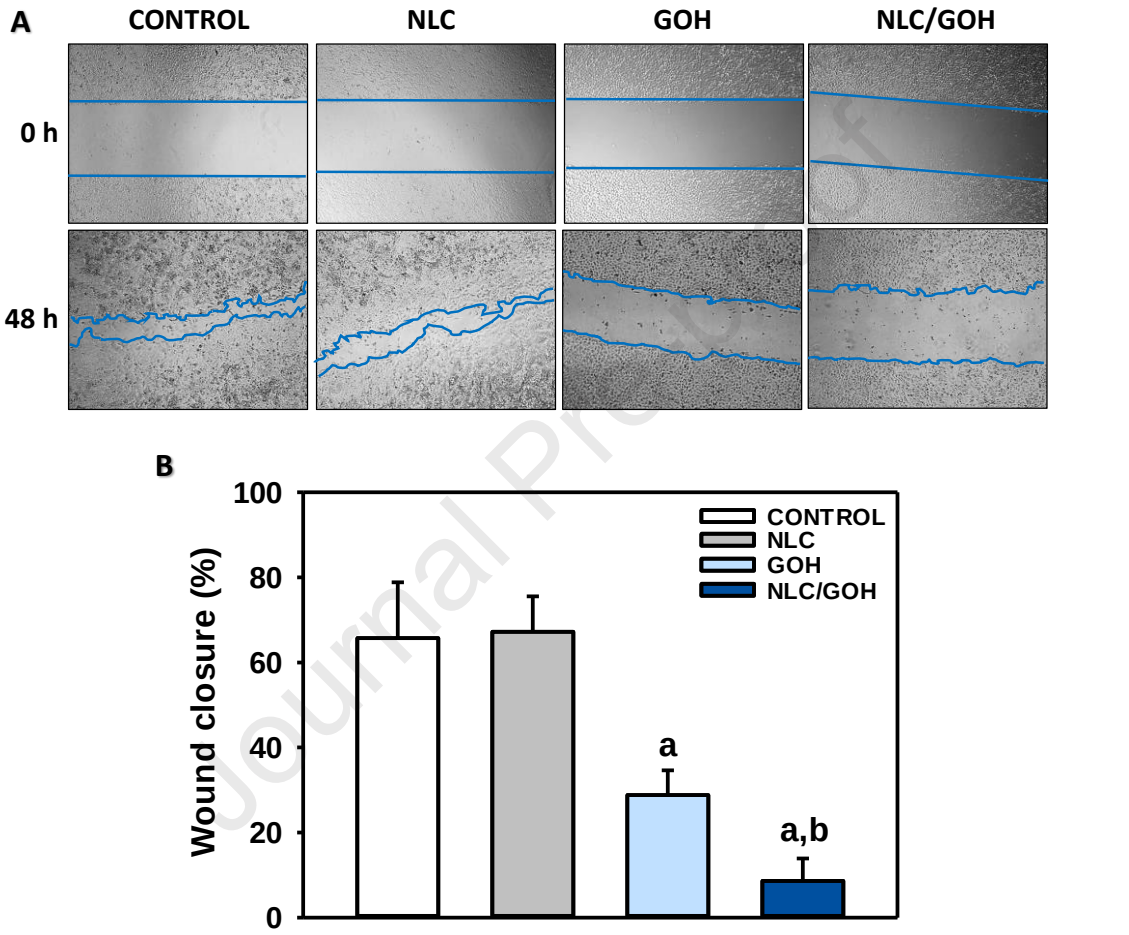

Figure 11. Encapsulation of GOH increases cell migration inhibition. The wound-healing assay was performed to analyze the migration of A549 cells following 0.1% DMSO (vehicle control), empty NLC, 1.0 mM free GOH, and 1.0 mM NLC/GOH exposure. (A) Representative images were obtained at 0 and 48 h (40 ×). (B) Quantitative analysis of wound healing closure. Data are presented as the mean ± SD (n=4). (a) $p < 0.001$ vs. control; (b) $p < 0.001$ vs. free GOH.

4. CONCLUSION

To our knowledge, this is the first report showing the improved anticancer activity of GOH after loading into lipid NPs. A high encapsulation efficiency of GOH into NLC was obtained, with NPs around 110 nm and very low dispersion (PDI< 0.2). The formulation was stable for at least 6 months after storage at 4 °C. SAXS/WAXS studies demonstrated that GOH could modify the crystallographic architecture of NLC, not only at the core but also at the interface level. An interesting pH dependence of GOH release from NLC was found, since 60% was released under physiological conditions but 100% was delivered at acid pH, simulating the tumoral environment after 24 h. No hemolysis of the formulation was observed. An increment of around 9 nm in the particle diameter was observed when the NLC/GOH formulation was incubated in FBS for 1 h, a finding that can be ascribed to the formation of a thin corona around the loaded nanovehicle but not to particle aggregation. The SPR studies predicted that NLC/GOH were prone to interact with HSA as compared with plasmatic opsonins, suggesting a potential long-term circulation of the NPs. The NLC/GOH were efficiently uptaken by A549 cells in a time-dependent manner after 24 h incubation. A significant 1.8 to 3.2-fold improvement in the anticancer activity of GOH was produced by nanoencapsulation. The mitochondrial membrane depolarization and cell death in A549 cells were exacerbated after the inclusion of GOH into NLC. Additionally, highly cytotoxic concentrations of NLC/GOH in A549 cells were not toxic in normal lung fibroblasts WI-38 cells. Furthermore, A549 cell migration inhibition induced by free GOH was increased when encapsulated in NLC. The present results demonstrate the potentiality of the NLC/GOH system as a promising carrier to improve cancer therapy.

Declaration of Competing Interest

The authors declare that they have no known competing financial interests or personal relationships that could have appeared to influence the work reported in this paper.

Acknowledgments

We appreciate the donations from Croda. This work was partially supported by UNLP (X041, X815, X861), CONICET (PIP 0034, PIP 0671), and ANPCyT (PICT 2016-1574, PICT 2017-2251, PICT 2016-4597; PICT 2017-0359; PICT2019-00199).

The authors thank Ms. Adriana Di Maggio for the careful English editing of the final version of this manuscript.

REFERENCES

[1] H. Sung, J. Ferlay, R.L. Siegel, M. Laversanne, I. Soerjomataram, A. Jemal, F. Bray, Global Cancer Statistics 2020: GLOBOCAN Estimates of Incidence and Mortality Worldwide for 36 Cancers in 185 Countries, CA Cancer J Clin. (2021).

[2] J. Ferlay, M. Colombet, I. Soerjomataram, D.M. Parkin, M. Piñeros, A. Znaor, F. Bray, Cancer statistics for the year 2020: An overview, Int J Cancer. 149 (2021) 778–789.

[3] H. Sung, J. Ferlay, R.L. Siegel, M. Laversanne, I. Soerjomataram, A. Jemal, F. Bray, Global cancer statistics 2020: GLOBOCAN estimates of incidence and mortality worldwide for 36 cancers in 185 countries, CA Cancer J Clin. 71 (2021) 209–249.

[4] E.C. Naylor, J.K. Desani, P.K. Chung, Targeted therapy and immunotherapy for lung cancer, Surgical Oncology Clinics. 25 (2016) 601–609.

[5] G.S. Shroff, P.M. de Groot, V.A. Papadimitrakopoulou, M.T. Truong, B.W. Carter, Targeted therapy and immunotherapy in the treatment of non–small cell lung cancer, Radiologic Clinics. 56 (2018) 485–495.

[6] L. Paz-Ares, T.-E. Ciuleanu, M. Cobo, M. Schenker, B. Zurawski, J. Menezes, E. Richardet, J. Bennouna, E. Felip, O. Juan-Vidal, First-line nivolumab plus ipilimumab combined with two cycles of chemotherapy in patients with non-small-cell lung cancer (CheckMate 9LA): an international, randomised, open-label, phase 3 trial, Lancet Oncol. 22 (2021) 198–211.

[7] P.M. Forde, J. Spicer, S. Lu, M. Provencio, T. Mitsudomi, M.M. Awad, E. Felip, S.R. Broderick, J.R. Brahmer, S.J. Swanson, Neoadjuvant nivolumab plus chemotherapy in resectable lung cancer, New England Journal of Medicine. (2022).

[8] D.J. Newman, G.M. Cragg, Natural products as sources of new drugs over the nearly four decades from 01/1981 to 09/2019, J Nat Prod. 83 (2020) 770–803.

[9] M. Huang, J.-J. Lu, J. Ding, Natural products in cancer therapy: past, present and future, Nat Prod Bioprospect. 11 (2021) 5–13.

[10] M.V. Sobral, A.L. Xavier, T.C. Lima, D.P. de Sousa, Antitumor activity of monoterpenes found in essential oils, The Scientific World Journal. 2014 (2014).

[11] W. Chen, A.M. Viljoen, Geraniol—a review of a commercially important fragrance material, South African Journal of Botany. 76 (2010) 643–651.

[12] W. Mączka, K. Wińska, M. Grabarczyk, One hundred faces of geraniol, Molecules. 25 (2020) 3303.

[13] M. Cho, I. So, J.N. Chun, J.-H. Jeon, The antitumor effects of geraniol: Modulation of cancer hallmark pathways, Int J Oncol. 48 (2016) 1772–1782.

[14] M. Galle, R. Crespo, B. Rodenak Kladniew, S. Montero Villegas, M. Polo, M.G. de Bravo, Suppression by geraniol of the growth of A549 human lung adenocarcinoma cells and inhibition of the mevalonate pathway in culture and in vivo: Potential use in cancer chemotherapy, Nutr Cancer. 66 (2014) 888–895.

[15] R. Crespo, B.E. Rodenak-Kladniew, M.A. Castro, M. v Soberón, S.M.L. Lavarías, Induction of oxidative stress as a possible mechanism by which geraniol affects the proliferation of human A549 and HepG2 tumor cells, Chem Biol Interact. 320 (2020) 109029.

[16] C. Turek, F.C. Stintzing, Stability of essential oils: a review, Compr Rev Food Sci Food Saf. 12 (2013) 40–53.

[17] C. Kohlert, I. van Rensen, R. März, G. Schindler, E.U. Graefe, M. Veit, Bioavailability and pharmacokinetics of natural volatile terpenes in animals and humans, Planta Med. 66 (2000) 495–505.

[18] D. Banerjee, S. Sengupta, Nanoparticles in cancer chemotherapy, Prog Mol Biol Transl Sci. 104 (2011) 489–507.

[19] A. Albanese, P.S. Tang, W.C.W. Chan, The effect of nanoparticle size, shape, and surface chemistry on biological systems, Annu Rev Biomed Eng. 14 (2012) 1–16.

[20] W. Mehnert, K. Mäder, Solid lipid nanoparticles: production, characterization and applications, Adv Drug Deliv Rev. 64 (2012) 83–101.

[21] G.A. Islan, M.L. Cacicedo, B. Rodenak-Kladniew, N. Duran, G.R. Castro, Development and Tailoring of Hybrid Lipid Nanocarriers, Curr Pharm Des. 23 (2018) 6643–6658.

[22] B. García-Pinel, C. Porras-Alcalá, A. Ortega-Rodríguez, F. Sarabia, J. Prados, C. Melguizo, J.M. López-Romero, Lipid-based nanoparticles: application and recent advances in cancer treatment, Nanomaterials. 9 (2019) 638.

[23] P. Piran, H.S. Kafil, S. Ghanbarzadeh, R. Safdari, H. Hamishehkar, Formulation of menthol-loaded nanostructured lipid carriers to enhance its antimicrobial activity for food preservation, Adv Pharm Bull. 7 (2017) 261.

[24] J.G. Galvão, R.L. Santos, A.R.S.T. Silva, J.S. Santos, A.M.B. Costa, H. Chandasana, V. v Andrade-Neto, E.C. Torres-Santos, A.A.M. Lira, S. Dolabella, Carvacrol loaded nanostructured lipid carriers as a promising parenteral formulation for leishmaniasis treatment, European Journal of Pharmaceutical Sciences. 150 (2020) 105335.

[25] B. Rodenak-Kladniew, N. Noacco, I. Pérez de Berti, S.J. Stewart, A.F. Cabrera, V.A. Alvarez, M. García de Bravo, N. Durán, G.R. Castro, G.A. Islan, Design of magnetic hybrid nanostructured lipid carriers containing 1,8-cineole as delivery systems for anticancer drugs: Physicochemical and cytotoxic studies, Colloids Surf B Biointerfaces. (2021).

[26] B. Rodenak-Kladniew, G.A. Islan, M.G. de Bravo, N. Durán, G.R. Castro, Design, characterization and in vitro evaluation of linalool-loaded solid lipid nanoparticles as potent tool in cancer therapy, Colloids Surf B Biointerfaces. 154 (2017) 123–132.

[27] B. Rodenak-Kladniew, S.S. Montoto, M.L. Sbaraglini, M. di Ianni, M.E. Ruiz, A. Talevi, V.A. Alvarez, N. Durán, G.R. Castro, G.A. Islan, Hybrid Ofloxacin/eugenol co-loaded solid lipid nanoparticles with enhanced and targetable antimicrobial properties, Int J Pharm. 569 (2019) 118575.

[28] D. Pozzi, G. Caracciolo, L. Digiacomo, V. Colapicchioni, S. Palchetti, A.L. Capriotti, C. Cavaliere, R.Z. Chiozzi, A. Puglisi, A. Laganà, The biomolecular corona of nanoparticles in circulating biological media, Nanoscale. 7 (2015) 13958–13966.

[29] B. Rodenak-Kladniew, M.A. Castro, R. Crespo, M. Galle, M. García de Bravo, Anti-cancer mechanisms of linalool and 1,8-cineole in non-small cell lung cancer A549 cells, Heliyon. (2020).

[30] I. Rivero Berti, B. Rodenak-Kladniew, C. Onaindia, C.G. Adam, G.A. Islan, N. Durán, G.R. Castro, Assessment of: In vitro cytotoxicity of imidazole ionic liquids and inclusion in targeted drug carriers containing violacein, RSC Adv. (2020).

[31] V. Jenning, A.F. Thünemann, S.H. Gohla, Characterisation of a novel solid lipid nanoparticle carrier system based on binary mixtures of liquid and solid lipids, Int J Pharm. 199 (2000) 167–177.

[32] K. Sato, Crystallization behaviour of fats and lipids—a review, Chem Eng Sci. 56 (2001) 2255–2265.

[33] S. Förster, A. Timmann, M. Konrad, C. Schellbach, A. Meyer, S.S. Funari, P. Mulvaney, R. Knott, Scattering curves of ordered mesoscopic materials, J Phys Chem B. 109 (2005) 1347–1360.

[34] N. Oh, J.-H. Park, Endocytosis and exocytosis of nanoparticles in mammalian cells, Int J Nanomedicine. 9 (2014) 51.

[35] B.A. Webb, M. Chimenti, M.P. Jacobson, D.L. Barber, Dysregulated pH: a perfect storm for cancer progression, Nat Rev Cancer. 11 (2011) 671–677.

[36] Y. Zhao, W. Ren, T. Zhong, S. Zhang, D. Huang, Y. Guo, X. Yao, C. Wang, W.-Q. Zhang, X. Zhang, Tumor-specific pH-responsive peptide-modified pH-sensitive liposomes containing doxorubicin for enhancing glioma targeting and anti-tumor activity, Journal of Controlled Release. 222 (2016) 56–66.

[37] S. Martins, S. Costa-Lima, T. Carneiro, A. Cordeiro-da-Silva, E.B. Souto, D.C. Ferreira, Solid lipid nanoparticles as intracellular drug transporters: an investigation of the uptake mechanism and pathway, Int J Pharm. 430 (2012) 216–227.

[38] M.J. Santander-Ortega, A.B. Jódar-Reyes, N. Csaba, D. Bastos-González, J.L. Ortega-Vinuesa, Colloidal stability of pluronic F68-coated PLGA nanoparticles: a variety of stabilisation mechanisms, J Colloid Interface Sci. 302 (2006) 522–529.

[39] C. Lourenco, M. Teixeira, S. Simões, R. Gaspar, Steric stabilization of nanoparticles: size and surface properties, Int J Pharm. 138 (1996) 1–12.

[40] A. Kovacevic, S. Savic, G. Vuleta, R.H. Mueller, C.M. Keck, Polyhydroxy surfactants for the formulation of lipid nanoparticles (SLN and NLC): effects on size, physical stability and particle matrix structure, Int J Pharm. 406 (2011) 163–172.

[41] C. Toledo, R.C. Gambaro, G. Padula, M.E. Vela, G.R. Castro, C.Y. Chain, G.A. Islan, Binary medical nanofluids by combination of polymeric Eudragit nanoparticles for vehiculization of tobramycin and resveratrol: antimicrobial, hemotoxicity and protein corona studies, J Pharm Sci. 110 (2021) 1739–1748.

[42] S.K. Chinnaiyan, D. Karthikeyan, V.R. Gadela, Development and characterization of metformin loaded pectin nanoparticles for T2 diabetes mellitus, Pharm Nanotechnol. 6 (2018) 253–263.

[43] H. Wang, Y. Lin, K. Nienhaus, G.U. Nienhaus, The protein corona on nanoparticles as viewed from a nanoparticle-sizing perspective, Wiley Interdiscip Rev Nanomed Nanobiotechnol. 10 (2018) e1500.

[44] J.K. Armstrong, R.B. Wenby, H.J. Meiselman, T.C. Fisher, The hydrodynamic radii of macromolecules and their effect on red blood cell aggregation, Biophys J. 87 (2004) 4259–4270.

[45] C. Carnovale, G. Bryant, R. Shukla, V. Bansal, Gold nanoparticle biodistribution and toxicity: Role of biological corona in relation with nanoparticle characteristics, in: Metal Nanoparticles in Pharma, Springer, 2017: pp. 419–436.

[46] M.J. Mitchell, M.M. Billingsley, R.M. Haley, M.E. Wechsler, N.A. Peppas, R. Langer, Engineering precision nanoparticles for drug delivery, Nat Rev Drug Discov. (2020) 1–24.

[47] M. Cho, I. So, J.N. Chun, J.-H. Jeon, The antitumor effects of geraniol: Modulation of cancer hallmark pathways, Int J Oncol. 48 (2016) 1772–1782.

[48] W. Mączka, K. Wińska, M. Grabarczyk, One Hundred Faces of Geraniol, Molecules. 25 (2020) 3303.

[49] S. Doktorovova, E.B. Souto, A.M. Silva, Nanotoxicology applied to solid lipid nanoparticles and nanostructured lipid carriers–a systematic review of in vitro data, European Journal of Pharmaceutics and Biopharmaceutics. 87 (2014) 1–18.

[50] T.-T.-L. Nguyen, V.-A. Duong, H.-J. Maeng, Pharmaceutical formulations with P-glycoprotein inhibitory effect as promising approaches for enhancing oral drug absorption and bioavailability, Pharmaceutics. 13 (2021) 1103.

[51] J. Halder, D. Pradhan, B. Kar, G. Ghosh, G. Rath, Nanotherapeutics approaches to overcome P-glycoprotein-mediated multi-drug resistance in cancer, Nanomedicine. (2021) 102494.

[52] G. Marslin, V. Khandelwal, G. Franklin, Cordycepin nanoencapsulated in poly (lactic-co-glycolic acid) exhibits better cytotoxicity and lower hemotoxicity than free drug, Nanotechnol Sci Appl. 13 (2020) 37.

[53] S. Fulda, L. Galluzzi, G. Kroemer, Targeting mitochondria for cancer therapy, Nat Rev Drug Discov. 9 (2010) 447.

[54] M. Riihimäki, H. Thomsen, K. Sundquist, J. Sundquist, K. Hemminki, Clinical landscape of cancer metastases, Cancer Med. 7 (2018) 5534–5542.

Author statement

Boris Rodenak-Kladniew: Investigation, Methodology, Formal analysis, Data curation, Validation, Project administration, Writing – review & editing, Funding acquisition

Rocío Gambaro: Investigation, Methodology, Formal analysis, Data curation.

José S. Cisneros: Investigation, Methodology, Conceptualization.

Cristián Huck-Iriart: Investigation, Methodology, Formal analysis, Conceptualization, Writing – review & editing.

Gisel Padula: Investigation, Methodology, Formal analysis, Conceptualization. Funding acquisition.

Guillermo R. Castro: Conceptualization, Writing – review & editing, Funding acquisition.

Cecilia Y. Chain: Investigation, Methodology, Conceptualization, Writing – review & editing.

Germán A. Islan: Conceptualization, Formal analysis, Project administration, Writing – review & editing, Funding acquisition.

Declaration of interests

☒ The authors declare that they have no known competing financial interests or personal relationships that could have appeared to influence the work reported in this paper.

☐The authors declare the following financial interests/personal relationships which may be considered as potential competing interests: